

Penetration Depth Evidence for Superconducting Gap Nodes in the Zone-Centered Hole Bands in KFe_2As_2

K. Hashimoto¹, A. Serafin², S. Tonegawa¹, R. Katsumata¹, R. Okazaki¹, T. Saito³, H. Fukazawa^{3,5}, Y. Kohori^{3,5}, K. Kihou^{4,5}, C. H. Lee^{4,5}, A. Iyo^{4,5}, H. Eisaki^{4,5}, H. Ikeda¹, Y. Matsuda¹, A. Carrington², and T. Shibauchi¹

¹Department of Physics, Kyoto University, Sakyo-ku, Kyoto 606-8502, Japan

²H. H. Wills Physics Laboratory, University of Bristol, Tyndall Avenue, Bristol, UK

³Department of Physics, Chiba University, Chiba 263-8522, Japan

⁴National Institute of Advanced Industrial Science and Technology (AIST), Tsukuba, Ibaraki 305-8568, Japan

⁵JST, Transformative Research-Project on Iron Pnictides (TRIP), Chiyoda, Tokyo 102-0075, Japan

(Dated: January 22, 2019)

Among the iron-based pnictide superconductors the material KFe_2As_2 is unusual in that its Fermi surface does not consist of quasi-nested electron and hole pockets. Here we report measurements of the temperature dependent London penetration depth of very clean crystals (residual resistivity ratio > 1200) of this compound. We show that the superfluid density at low temperatures exhibits a strong linear-in-temperature dependence which implies that there are line nodes in the energy gap on the large zone-centered hole sheets. The results indicate that KFe_2As_2 is an unconventional superconductor with strong electron correlations.

The discovery of high transition temperature (T_c) iron-based superconductors (IBS) raises fundamental questions about origin of superconductivity [1]. The microscopic pairing interactions with give rise to superconductivity are intimately related to the structure of the superconducting energy gap which may be probed experimentally by studying the nature of the low-energy quasiparticle excitations. In particular, the presence of nodes in the energy gap signals an unconventional pairing mechanism, and the position of the nodes can be a strong guide as the exact form of the pairing interaction V'_{kk} .

Based on analyses of spin-fluctuation mediated pairing models, several different gap structures have been proposed [2–6]. The rich variety of possible pairing states has as its origin the unusual multiband electronic structure of the IBS. In most IBS there are disconnected quasi-two-dimensional hole and electron Fermi-surface sheets. The former are centered on the Γ point in the Brillouin zone and the latter at the zone corner. It has been proposed that strong scattering between the electron and hole sheets, corresponding to a wavevector $q \sim (\pi, \pi)$ leads to a nodeless gap with sign change between the hole and electron sheets (nodeless s_{\pm} state). However, if in addition to this there is strong low q scattering this can stabilize a state with nodes in the electron and/or hole bands with either s or d -wave symmetry. c -axis Fermi-surface dispersion could also generate horizontal line nodes [7].

Thus far experimental studies have given evidence for two distinct types of nodal structure in IBS [1]: one is nodeless but may have significant anisotropy [8–13] and the other has line nodes [14–18]. The former fully gapped state seems consistent with the nodeless s_{\pm} state [19]. For the latter case, unambiguous evidence of nodal lines has been obtained from the penetration depth and thermal conductivity measurements in the compensated metals LaFePO ($T_c = 6$ K) and $\text{BaFe}_2(\text{As},\text{P})_2$ ($T_c = 30$ K). In both materials, recent studies [16, 20, 21] suggest that the nodes are most likely located on the electron bands near the zone corner of the Brillouin Zone, and that the hole bands centered at the Γ point remains fully

gapped.

To uncover how the superconducting gap structure is related to the microscopic pairing in IBS, studies of KFe_2As_2 may be particularly instructive. This superconductor has a relatively low $T_c \simeq 3$ K and is the end member of the $(\text{Ba}_{1-x}\text{K}_x)\text{Fe}_2\text{As}_2$ series. Unlike most other IBS where the volumes of the electron and hole sheets are roughly equal, in KFe_2As_2 the volumes differ by one electron per unit cell. This causes a substantial change in the Fermi surface topology. As shown in Fig. 1, the ubiquitous X centered electron sheets are replaced by small quasi-two-dimensional hole-like tubes which do not nest at all with the Γ -centered hole sheets. If nesting does play an important role in the superconductivity of the high T_c IBS then the nature of the superconducting state should be quite different in KFe_2As_2 . It is also intriguing that the electronic specific heat is quite large ($\gamma = 93 \text{ mJ/K}^2\text{mol}$) compared with other IBS [22], suggesting the importance of electron correlations in KFe_2As_2 . In this paper, we report measurements of the temperature dependent penetration depth of KFe_2As_2 which shows that this material has well formed line nodes located in the Γ centered hole bands.

The single crystals were grown by a K-flux method [22]. The temperature dependence of the magnetic penetration

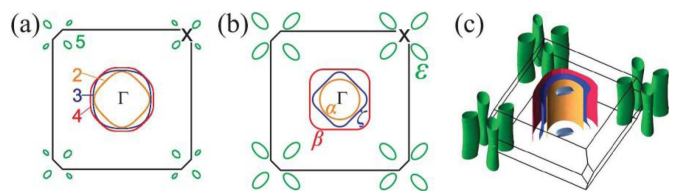


FIG. 1. (Color online). The Fermi surface of KFe_2As_2 (labels in correspond to Table I). (a) 2D cross-sectional representation of our band-structure calculations (note the pillow surface from band 1 does not appear in this cut), (b) Schematic cross-section with shapes of the various pockets determined by dHvA [35] and ARPES [34] experiments. (c) 3D view of band-structure calculated Fermi surface with bands shifted to best fit the dHvA data.

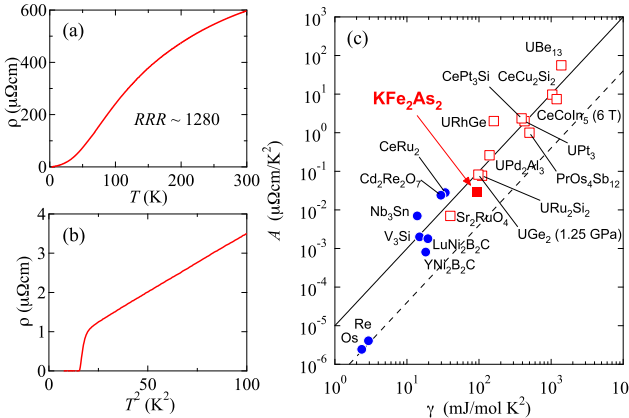


FIG. 2. (Color online). (a) Temperature dependence of in-plane resistivity $\rho(T)$ in a single crystal of KFe_2As_2 . (b) The same data plotted against T^2 below 10 K. (c) Coefficient A vs Sommerfeld constant γ (Kadowaki-Woods plot [37]) for various superconductors showing the Fermi-liquid AT^2 dependence of resistivity. Blue circles are for s -wave superconductors, while red squares are for unconventional superconductors with nodes in the gap. The lines represent $A = a_{\text{KW}}\gamma^2$, with $a_{\text{KW}} = 10^{-5}$ (solid line) and $4 \times 10^{-7} \mu\Omega\text{cm}(\text{Kmol}/\text{mJ})^2$ (dashed line).

depth was measured using a tunnel-diode oscillator in a dilution refrigerator [14]. The ac magnetic field is applied parallel to the c axis so that the shielding currents flow in the ab -plane. To avoid degradation of the crystals due to reaction with air moisture, we cleaved the crystals on all six sides while they were coated in a thick layer of grease. The measurements were done just after the cleavage without exposure in air. The relatively sharp superconducting transitions found in the frequency shift of the oscillator as well as in the specific heat measured after the penetration depth measurements [inset of Fig. 3(a)] indicate that our procedure does not damage the sample quality.

Dc resistivity $\rho(T)$ measurements show that our crystals are extremely clean with the residual resistivity ratio $RRR = \rho(300 \text{ K})/\rho_0$ of 1280 [Figs. 2(a) and (b)]. The low-temperature normal-state $\rho(T)$ follows the Fermi-liquid dependence $\rho_0 + AT^2$ with $A = 0.030(7) \mu\Omega\text{cm}/\text{K}^2$ [23], and the residual resistivity ρ_0 is estimated by extrapolation. We note our data is not consistent with the non-Fermi-liquid $T^{1.5}$ behavior reported by Dong *et al.* for samples with much lower RRR (~ 100) [24], but is consistent with another previous report [25]. The obtained relatively large A value follows the Kadowaki-Woods relation $A = a_{\text{KW}}\gamma^2$, with $a_{\text{KW}} \approx 10^{-5} \mu\Omega\text{cm}(\text{Kmol}/\text{mJ})^2$, indicating that strongly correlated electrons with large mass are responsible for the Fermi-liquid T^2 dependence. As demonstrated in Fig. 2(c), KFe_2As_2 is at the edge of heavy-fermion superconductors with nodes in the energy gap which are widely believed to have unconventional mechanisms of superconductivity.

Figure 3(a) shows the low-temperature variation of the change in the penetration depth $\Delta\lambda(T) = \lambda(T) - \lambda(0)$ in two samples. In both samples a strong T -linear dependence is ob-

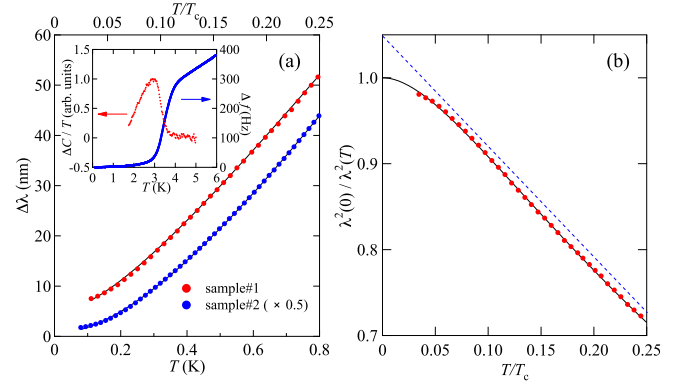


FIG. 3. (Color online). (a) Change in the penetration depth $\Delta\lambda(T)$ at low temperatures in two samples. The data are shifted vertically for clarity. Inset shows the frequency shift Δf of the tunnel diode oscillator containing sample 1 (blue) and relative change in the specific heat C divided by temperature $\Delta C/T$ in the same sample (red). C was measured using a modulated temperature method [38]. (b) Normalized superfluid density at low temperatures follows a T -linear dependence (dashed line). Here we used $\lambda(0) = 260 \text{ nm}$ estimated from the Fermi-surface parameters (see Table I). The solid lines are fits to the empirical formula involving the impurity scattering in superconductors with line nodes (see text).

served over a wide temperature range of $0.1 \lesssim T/T_c \lesssim 0.3$. Such strong T -linear dependence is distinctly different from the exponential dependence expected in the fully-gapped superconducting state and is instead consistent with gap with well-developed line nodes. A linear temperature dependence can only be explained by the presence of line nodes. This is in contrast to power law behaviors with exponents close to 2 which could be consistent either with nodal behavior in the dirty limit or with strong impurity scattering in (for example) the intrinsically fully gapped s_{\pm} state [26]. Evidence for line nodes in this compound has also been found in NMR, specific heat [27] and thermal conductivity [24] measurements.

Deviations from the T -linear behavior of $\lambda(T)$ are observed at the lowest temperatures which are likely due to a finite zero-energy density of states created by a small amount of impurity scattering. When impurity scattering is present in superconductors with line nodes, the low-temperature $\Delta\lambda(T)$ changes from T to T^2 , as observed in Zn-doped $\text{YBa}_2\text{Cu}_3\text{O}_7$ [28]. The temperature below which the T^2 behavior is observed depends on the levels of disorder, which can be described by the empirical formula as $\Delta\lambda(T) \propto T^2/(T + T^*)$ [29]. A fit to this formula [solid lines in Fig. 3] gives $T^* \approx 0.3 \text{ K}$ for sample 1 and $T^* \approx 0.5 \text{ K}$ for sample 2, which indicates relatively small levels of disorder in these crystals. Although the temperature dependence of λ is consistent between samples the absolute values of $d\lambda/dT$ differ by a factor two. This is likely due to roughness of the cut edges of the samples and the lower value (sample # 1) is likely to be more representative of the intrinsic value.

To evaluate the normalized superfluid density $n_s(T)/n_s(0) = \lambda^2(0)/\lambda^2(T)$, we need the value of

TABLE I. Contributions of each band to the normalized superfluid density $\lambda^2(0)/\lambda^2(T)$ evaluated from DFT band structure calculations as well as the dHvA measurements [35]. m_e is the free electron mass.

From DFT calculations					From dHvA			
Sheet	# holes	DOS (/eV)	ω_p (eV)	$\frac{\omega_p^2}{(\omega_p^2)_{\text{total}}}$ (%)	name	# holes	$\frac{m^*}{m_e}$	$\frac{\omega_p^2}{(\omega_p^2)_{\text{total}}}$ (%)
1 (pillow at Z)	0.002	0.055	0.16	0.4	—	—	—	—
2 (inner tube at Γ)	0.258	1.11	1.466	32	α	0.17	6	31
3 (middle tube at Γ)	0.342	1.48	1.3959	29	ζ	0.26	13	23
4 (outer tube at Γ)	0.390	1.52	1.5098	34	β	0.48	18	31
5 (tubes near X)	0.009	1.328	0.55	5	ε	0.09	7	15
total	1.00	5.494	2.577	100		1.0		100

$\lambda(0)$, which we cannot measure directly in our experiment. Recent small-angle neutron scattering (SANS) measurements [30] estimate $\lambda(T = 55 \text{ mK}) \approx 200 \text{ nm}$ and μSR measurements [31] give $\lambda(T_c/2) \approx 280 \text{ nm}$ which also suggests $\lambda(0) \sim 200 \text{ nm}$. These values are close to the $\lambda(0)$ values calculated from the Fermi surface parameters [see Table I]. Regardless of the choice of $\lambda(0)$ value within these uncertainties, the obtained temperature dependence of $n_s(T)$ shows a T -linear behavior over a even wider range of T than $\lambda(T)$ itself [Figs. 3(b) and 4]. This is expected from theory as for a nodal superconductor the non-linear corrections to $n_s(T)$ are significant smaller than those for $\lambda(T)$. Hence it is expected that the limiting low temperature behavior of $n_s(T)$ survives to higher temperature than that of $\lambda(T)$.

In order to proceed with a more quantitative analysis of our results we have estimated the contribution of each of the Fermi surface sheets to the total superfluid density. As a first approach we have calculated the band-structure of KFe₂As₂ using density functional theory (DFT) using the WIEN2K package [32] and the experimental lattice constants and internal positions [33]. 4×10^5 k -points (in the full Brillouin zone) were used for the calculations of plasma frequencies ω_p , Fermi surface volumes and sheet specific density of states (DOS) which are reported in Table I. The Fermi surface topology and band masses are very similar to those reported previously [25] (see Fig. 1). The calculated total DOS and ω_p correspond to the Sommerfeld constant $\gamma = 13.0 \text{ mJ/K}^2\text{mol}$ and $\lambda(0) = 76.6 \text{ nm}$, respectively. The experimentally observed $\gamma = 93 \text{ mJ/K}^2\text{mol}$ [22] implies a renormalization of 7.2, which would increase $\lambda(0)$ to 205 nm.

Although the general feature of this Fermi surface calculation are confirmed by photoemission (ARPES) [34] and de Haas-van Alphen (dHvA) measurements [35], the exact size of the various sheets and their warping are not. Also, dHvA measurements show that the mass renormalization effects vary between the different sheets. So as a second approach we estimate the contribution of the various sheets to the superfluid density directly from the dHvA measurements, assuming each sheet is a simple two dimensional cylinder. As the largest β sheet (see Fig. 1) was not observed by dHvA, we estimate its contribution by estimating its total volume from the constraint that total number of holes must equal unity and its mass from the difference between the measured specific heat and the contributions from the observed sheets. Note that for sheets with more than one extremal dHvA orbit we have

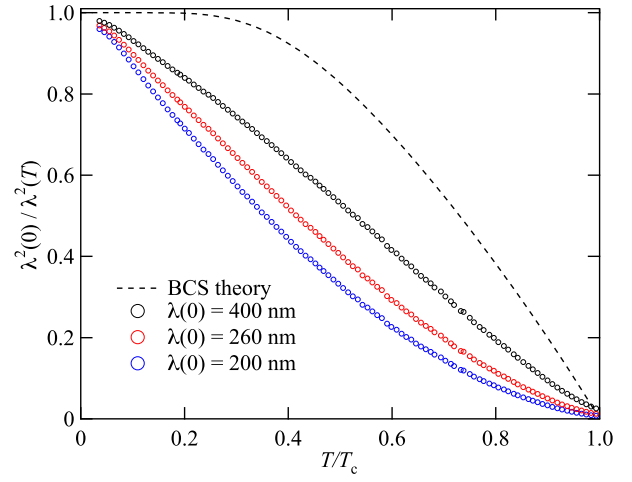


FIG. 4. (Color online). Normalized superfluid density obtained by using representative values of $\lambda(0)$. The dashed line is the BCS temperature dependence in a fully gapped superconductor.

taken the average mass / cross-sectional area. Also we have ignored any possible contribution from the small pillow sheet (band 1) as this was not observed by dHvA and in any case would make only a very small contribution. The contribution of each sheet to the superfluid density were then calculated using $\lambda^{-2} = \mu_0 e^2 n_H / m^* = \omega_p^2 / c^2$, where n_H and m^* are the hole density and effective mass for each sheet. From this we obtain a total superfluid density which corresponds to $\lambda(0) = 260 \text{ nm}$. The fact that this procedure and the direct calculation from the band-structure give value of $\lambda(0)$ which compare favorable to the direct measurements by μSR and SANS gives us confidence in the accuracy of the result. The good accord between the two estimates despite the difference between the calculated Fermi surface cross-sections and the dHvA experiments is not surprising as the DOS is independent of Fermi surface size in two-dimensions. A key result from this analysis is that the contribution of the the ε band near the X point is small. It contributes only up to $\sim 15\%$ of the total superfluid density.

The temperature dependence of the normalized superfluid density $\lambda^2(0)/\lambda^2(T)$ is plotted in Fig. 4. Here we have used

two representative value of $\lambda(0)$ which encompass the values from SANS/ μ SR measurements and the above estimates from Fermi surface parameters, as well as a factor of 2 longer case $\lambda(0) = 400$ nm than the SANS/ μ SR estimate which would set an upper limit of uncertainties. These plots indicate that the superfluid density at $T = T_c/3$ does not exceed $\sim 75\%$ of the zero-temperature value. This requires that nodes are located on at least one of the Γ -centered bands which have large contributions to the superfluid density. The ε band can have only a small contribution as they only contribute $\sim 15\%$ to the total superfluid density.

As demonstrated in Fig. 2(c), in superconductors with strong electron correlations where the A and γ values are strongly enhanced, Cooper pairs with finite angular momentum (p , d -wave, etc.) are favorable as these states reduce the Coulomb repulsion. Our results indicate that KFe₂As₂ with γ and A values comparable to some heavy-fermion superconductors has well-developed line nodes in the zone-centered large bands. This implies that the electron correlations play an important role in this compound and that an electronic (non-phononic) pairing mechanism is needed to overcome the Coulomb repulsion. Since the Γ -centered sheets in

KFe₂As₂ are relatively large, it is likely that the intra-band spin-fluctuations are important to create the sign change inside these bands, which gives rise to line nodes. Recent theoretical calculations [36] reveal that the spin susceptibility in heavily hole doped system has relatively weak momentum dependence, which suggests the relative importance of scattering vectors other than $\mathbf{q} \sim (\pi, \pi)$.

In summary, we have measured the London penetration depth in very clean crystals of highly hole doped IBS KFe₂As₂. A strong T -linear behavior is found in the superfluid density at low temperatures, indicative of line nodes in the gap function. Quantitative analysis of the contributions of each band to the superfluid density shows that the line nodes are located in the Γ -centered bands, pointing to an unconventional mechanism of superconductivity and strong electron correlations in this system.

We thank discussions with E. M. Forgan, S. Kasahara, H. Kawano-Furukawa, K. Kuroki, K. Ohishi, and T. Terashima. This work is supported by KAKENHI from JSPS, Grant-in-Aid for GCOE program “The Next Generation of Physics, Spun from Universality and Emergence” from MEXT, Japan, and EPSRC in the UK.

[1] K. Ishida, Y. Nakai, and H. Hosono, *J. Phys. Soc. Jpn.* **78**, 062001 (2009).
[2] I. I. Mazin, D. J. Singh, M. D. Johannes, and M. H. Du, *Phys. Rev. Lett.* **101**, 057003 (2008).
[3] K. Kuroki, H. Usui, S. Onari, R. Arita, and H. Aoki, *Phys. Rev. B* **79**, 224511 (2009).
[4] A. V. Chubukov, M. G. Vavilov, and A. B. Vorontsov, *Phys. Rev. B* **80**, 140515(R) (2009).
[5] S. Graser *et al.*, *New J. Phys.* **11**, 025016 (2009); arXiv:1003.0133.
[6] H. Ikeda, R. Arita, and J. Kuneš, *Phys. Rev. B* **81**, 054502 (2010).
[7] K. Kuroki (private communications).
[8] K. Hashimoto *et al.*, *Phys. Rev. Lett.* **102**, 017002 (2009); *Phys. Rev. Lett.* **102**, 207001 (2009).
[9] L. Malone *et al.*, *Phys. Rev. B* **79**, 140501(R) (2009).
[10] H. Ding *et al.*, *Europhys. Lett.* **83**, 47001 (2008).
[11] H. Kim *et al.*, arXiv:1003.2959; R. T. Gordon *et al.*, arXiv:0912.5346, and references therein.
[12] M. Yamashita *et al.*, *J. Phys. Soc. Jpn.* **78**, 103702 (2009).
[13] X. G. Luo *et al.*, *Phys. Rev. B* **80**, 140503(R) (2009); M. A. Tanatar *et al.*, *Phys. Rev. Lett.* **104**, 067002 (2010); L. Ding *et al.*, *New J. Phys.* **11**, 093018 (2009).
[14] J. D. Fletcher *et al.*, *Phys. Rev. Lett.* **102**, 147001 (2009).
[15] C. W. Hicks *et al.*, *Phys. Rev. Lett.* **103**, 127003 (2009).
[16] M. Yamashita *et al.*, *Phys. Rev. B* **80**, 220509(R) (2009).
[17] K. Hashimoto *et al.*, arXiv:0907.4399.
[18] Y. Nakai *et al.*, *Phys. Rev. B* **81**, 020503(R) (2010).
[19] H. Kontani and S. Onari, arXiv:0912.1975.
[20] J. S. Kim *et al.*, arXiv:1002.3355.
[21] T. Shimojima *et al.* (unpublished).
[22] H. Fukazawa *et al.* (unpublished).
[23] Au contacts evaporated after Ar plasma cleaning of the surface give contact resistance less than 1Ω . The main source of errors in the absolute value of ρ is the separation between voltage contacts which have finite widths.
[24] J. K. Dong *et al.*, *Phys. Rev. Lett.* **104**, 087005 (2010).
[25] T. Terashima *et al.*, *J. Phys. Soc. Jpn.* **78**, 063702 (2009).
[26] A. B. Vorontsov, M. G. Vavilov, and A. V. Chubukov, *Phys. Rev. B* **79**, 140507(R) (2009); Y. Bang, *EPL* **86**, 47001 (2009).
[27] H. Fukazawa *et al.*, *J. Phys. Soc. Jpn.* **78** 083712 (2009).
[28] D. A. Bonn *et al.*, *Phys. Rev. B* **50**, 4051 (1994).
[29] P. J. Hirschfeld, and N. Goldenfeld, *Phys. Rev. B* **48**, 4219 (1993).
[30] H. Kawano-Furukawa *et al.* (unpublished).
[31] K. Ohishi *et al.* (unpublished).
[32] P. Blaha *et al.*, “An augmented plane wave and local orbitals program for calculating crystal properties” (Technical University of Wien, Vienna, 2001).
[33] S. Rozca, and H. U. Schuster, *Z. Naturforsch. B* **36**, 1668 (1981). $a = 3.841\text{ \AA}$, $c = 13.861\text{ \AA}$, and $z_{\text{As}} = 0.3525$.
[34] T. Sato *et al.*, *Phys. Rev. Lett.* **103**, 047002 (2009).
[35] T. Terashima *et al.*, arXiv:1001.3441.
[36] H. Ikeda, R. Arita, and J. Kuneš, arXiv:1002.4471.
[37] Y. Kasahara *et al.*, *Phys. Rev. Lett.* **96**, 247004 (2006).
[38] A. Carrington *et al.*, *Phys. Rev. B* **55**, R8674 (1997).